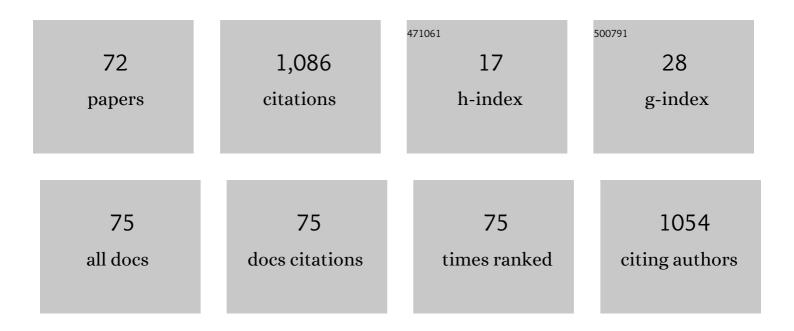
Bernard Chiu

List of Publications by Year in descending order

Source: https://exaly.com/author-pdf/113528/publications.pdf Version: 2024-02-01



REDNADD CHILL

#	Article	IF	CITATIONS
1	Multilabel Classification With Group-Based Mapping: A Framework With Local Feature Selection and Local Label Correlation. IEEE Transactions on Cybernetics, 2022, 52, 4596-4610.	6.2	12
2	Cascaded Triplanar Autoencoder M-Net for Fully Automatic Segmentation of Left Ventricle Myocardial Scar From Three-Dimensional Late Gadolinium-Enhanced MR Images. IEEE Journal of Biomedical and Health Informatics, 2022, 26, 2582-2593.	3.9	13
3	Segmentation of common and internal carotid arteries from 3D ultrasound images based on adaptive triple loss. Medical Physics, 2021, 48, 5096-5114.	1.6	12
4	Three-dimensional ultrasound assessment of effects of therapies on carotid atherosclerosis using vessel wall thickness maps. Ultrasound in Medicine and Biology, 2021, 47, 2502-2513.	0.7	10
5	Three-dimensional ultrasound evaluation of the effects of pomegranate therapy on carotid plaque texture using locality preserving projection. Computer Methods and Programs in Biomedicine, 2020, 184, 105276.	2.6	12
6	Longitudinal assessment of carotid plaque texture in three-dimensional ultrasound images based on semi-supervised graph-based dimensionality reduction and feature selection. Computers in Biology and Medicine, 2020, 116, 103586.	3.9	11
7	Segmentation of 3D ultrasound carotid vessel wall using U-Net and segmentation average network. , 2020, 2043-2046.		13
8	Identification of Retinal Ganglion Cells from β-III Stained Fluorescent Microscopic Images. Journal of Digital Imaging, 2020, 33, 1352-1363.	1.6	2
9	Deep-recursive residual network for image semantic segmentation. Neural Computing and Applications, 2020, 32, 12935-12947.	3.2	17
10	Area-Preserving Mapping of 3D Carotid Ultrasound Images Using Density-Equalizing Reference Map. IEEE Transactions on Biomedical Engineering, 2020, 67, 2507-2517.	2.5	15
11	Vessel wall segmentation of common carotid artery via multi-branch light network. , 2020, , .		9
12	Plaque components segmentation in carotid artery on simultaneous non-contrast angiography and intraplaque hemorrhage imaging using machine learning. Magnetic Resonance Imaging, 2019, 60, 93-100.	1.0	18
13	A self-tuned graph-based framework for localization and grading prostate cancer lesions: An initial evaluation based on multiparametric magnetic resonance imaging. Computers in Biology and Medicine, 2018, 96, 252-265.	3.9	3
14	Breast lesion classification based on supersonic shear-wave elastography and automated lesion segmentation from B-mode ultrasound images. Computers in Biology and Medicine, 2018, 93, 31-46.	3.9	26
15	Carotid plaque segmentation from three-dimensional ultrasound images by direct three-dimensional sparse field level-set optimization. Computers in Biology and Medicine, 2018, 94, 27-40.	3.9	14
16	Trace Ratio Criterion based Discriminative Feature Selection via l2,-norm regularization for supervised learning. Neurocomputing, 2018, 321, 1-16.	3.5	19
17	Prostate lesion delineation from multiparametric magnetic resonance imaging based on locality alignment discriminant analysis. Medical Physics, 2018, 45, 4607-4618.	1.6	6

18 AWM: Adaptive Weight Matting for medical image segmentation. , 2017, , .

BERNARD CHIU

#	Article	IF	CITATIONS
19	Conformal mapping of carotid vessel wall and plaque thickness measured from 3D ultrasound images. Medical and Biological Engineering and Computing, 2017, 55, 2183-2195.	1.6	16
20	Simulation Study of an Ultrasound Retinal Prosthesis With a Novel Contact-Lens Array for Noninvasive Retinal Stimulation. IEEE Transactions on Neural Systems and Rehabilitation Engineering, 2017, 25, 1605-1611.	2.7	14
21	Prostate lesion detection and localization based on locality alignment discriminant analysis. Proceedings of SPIE, 2017, , .	0.8	3
22	Longitudinal Analysis of Pre-Term Neonatal Cerebral Ventricles From 3D Ultrasound Images Using Spatial-Temporal Deformable Registration. IEEE Transactions on Medical Imaging, 2017, 36, 1016-1026.	5.4	8
23	Sensitive threeâ€dimensional ultrasound assessment of carotid atherosclerosis by weighted average of local vessel wall and plaque thickness change. Medical Physics, 2017, 44, 5280-5292.	1.6	15
24	Automatic segmentation approach to extracting neonatal cerebral ventricles from 3D ultrasound images. Medical Image Analysis, 2017, 35, 181-191.	7.0	38
25	A Graph-Based Multi-kernel Feature Weight Learning Framework for Detection and Grading of Prostate Lesions Using Multi-parametric MR Images. , 2017, , .		0
26	Accurate quantification of local changes for carotid arteries in 3D ultrasound images using convex optimization-based deformable registration. Proceedings of SPIE, 2016, , .	0.8	3
27	Direct 3D segmentation of carotid plaques from 3D ultrasound images. , 2016, , .		0
28	Correspondence optimization in 2D standardized carotid wall thickness map by description length minimization: A tool for increasing reproducibility of 3D ultrasoundâ€based measurements. Medical Physics, 2016, 43, 6474-6490.	1.6	8
29	Fully automatic prostate segmentation from transrectal ultrasound images based on radial bas-relief initialization and slice-based propagation. Computers in Biology and Medicine, 2016, 74, 74-90.	3.9	10
30	Three-dimensional ultrasound measurements of carotid vessel wall and plaque thickness and their relationship with pulmonary abnormalities in ex-smokers without airflow limitation. International Journal of Cardiovascular Imaging, 2016, 32, 1391-1402.	0.7	7
31	Concise biomarker for spatial–temporal change in three-dimensional ultrasound measurement of carotid vessel wall and plaque thickness based on a graph-based random walk framework: Towards sensitive evaluation of response to therapy. Computers in Biology and Medicine, 2016, 79, 149-162.	3.9	6
32	Modeling hemodynamic forces in carotid artery based on local geometric features. Medical and Biological Engineering and Computing, 2016, 54, 1437-1452.	1.6	6
33	A framework for quantification and visualization of segmentation accuracy and variability in 3D lateral ventricle ultrasound images of preterm neonates. Medical Physics, 2015, 42, 6387-6405.	1.6	1
34	Fast segmentation of the femoral arteries from 3D MR images: A tool for rapid assessment of peripheral arterial disease. Medical Physics, 2015, 42, 2431-2448.	1.6	5
35	Quantification of cerebral ventricle volume change of preterm neonates using 3D ultrasound images. , 2015, , .		1
36	3D MR ventricle segmentation in pre-term infants with post-hemorrhagic ventricle dilation. Proceedings of SPIE, 2015, , .	0.8	0

BERNARD CHIU

#	Article	IF	CITATIONS
37	3D MR ventricle segmentation in pre-term infants with post-hemorrhagic ventricle dilatation (PHVD) using multi-phase geodesic level-sets. NeuroImage, 2015, 118, 13-25.	2.1	19
38	Feasibility of Multiple Micro-Particle Trapping—A Simulation Study. Sensors, 2015, 15, 4958-4974.	2.1	0
39	Joint segmentation of lumen and outer wall from femoral artery MR images: Towards 3D imaging measurements of peripheral arterial disease. Medical Image Analysis, 2015, 26, 120-132.	7.0	8
40	Automatic prostate segmentation from transrectal ultrasound images. , 2014, , .		4
41	Assessment of femoral artery atherosclerosis at the adductor canal using 3D black-blood MRI. Clinical Radiology, 2013, 68, e213-e221.	0.5	5
42	Quantification and visualization of carotid segmentation accuracy and precision using a 2D standardized carotid map. Physics in Medicine and Biology, 2013, 58, 3671-3703.	1.6	21
43	A framework for the co-registration of hemodynamic forces and atherosclerotic plaque components. Physiological Measurement, 2013, 34, 977-990.	1.2	10
44	Novel 3D ultrasound image-based biomarkers based on a feature selection from a 2D standardized vessel wall thickness map: a tool for sensitive assessment of therapies for carotid atherosclerosis. Physics in Medicine and Biology, 2013, 58, 5959-5982.	1.6	19
45	Relationships between local geometrical features and hemodynamic flow properties. , 2013, 2013, 723-6.		1
46	Joint Segmentation of 3D Femoral Lumen and Outer Wall Surfaces from MR Images. Lecture Notes in Computer Science, 2013, 16, 534-541.	1.0	2
47	Characterization of Carotid Plaques on 3-Dimensional Ultrasound Imaging by Registration With Multicontrast Magnetic Resonance Imaging. Journal of Ultrasound in Medicine, 2012, 31, 1567-1580.	0.8	22
48	Fast plaque burden assessment of the femoral artery using 3D black-blood MRI and automated segmentation. Medical Physics, 2011, 38, 5370-5384.	1.6	24
49	3D Carotid Ultrasound Imaging. , 2011, , 325-350.		4
50	Carotid Plaque Surface Irregularity. , 2011, , 279-297.		0
51	Three-Dimensional Carotid Ultrasound Segmentation Variability Dependence on Signal Difference and Boundary Orientation. Ultrasound in Medicine and Biology, 2010, 36, 95-110.	0.7	9
52	Optimal processing of isotropic 3D black-blood MRI For accurate estimation of vessel wall thickness. , 2010, , .		0
53	Correlation of hemodynamic forces and atherosclerotic plaque components. , 2010, , .		2
54	Analysis of carotid lumen surface morphology using three-dimensional ultrasound imaging. Physics in Medicine and Biology, 2009, 54, 1149-1167.	1.6	28

Bernard Chiu

#	Article	IF	CITATIONS
55	Magnetic resonance imaging and threeâ€dimensional ultrasound of carotid atherosclerosis: Mapping regional differences. Journal of Magnetic Resonance Imaging, 2009, 29, 901-908.	1.9	18
56	Three-dimensional Ultrasound Quantification of Intensive Statin Treatment of Carotid Atherosclerosis. Ultrasound in Medicine and Biology, 2009, 35, 1763-1772.	0.7	87
57	A surface-based metric for registration error quantification. , 2009, , .		3
58	Nonrigid registration of threeâ€dimensional ultrasound and magnetic resonance images of the carotid arteries. Medical Physics, 2009, 36, 373-385.	1.6	22
59	Development of 3D ultrasound techniques for carotid artery disease assessment and monitoring. International Journal of Computer Assisted Radiology and Surgery, 2008, 3, 1-10.	1.7	14
60	Area-preserving flattening maps of 3D ultrasound carotid arteries images. Medical Image Analysis, 2008, 12, 676-688.	7.0	28
61	Mapping Spatial and Temporal Changes in Carotid Atherosclerosis from Three-Dimensional Ultrasound Images. Ultrasound in Medicine and Biology, 2008, 34, 64-72.	0.7	35
62	Quantification of carotid arteries atherosclerosis using 3D ultrasound images and area-preserving flattened maps. Proceedings of SPIE, 2008, , .	0.8	0
63	A "Twisting and Bending―Model-Based Nonrigid Image Registration Technique for 3-D Ultrasound Carotid Images. IEEE Transactions on Medical Imaging, 2008, 27, 1378-1388.	5.4	17
64	Quantification of carotid vessel wall and plaque thickness change using 3D ultrasound images. Medical Physics, 2008, 35, 3691-3710.	1.6	68
65	Nonrigid registration of carotid ultrasound and MR images using a "twisting and bending" model. , 2008, , .		2
66	Fast prostate segmentation in 3D TRUS images based on continuity constraint using an autoregressive model. Medical Physics, 2007, 34, 4109-4125.	1.6	38
67	Quantification of progression and regression of carotid vessel atherosclerosis using 3D ultrasound images. , 2006, 2006, 3819-22.		9
68	Quantification of carotid vessel atherosclerosis. , 2006, 6143, 85.		10
69	Prostate contouring uncertainty in megavoltage computed tomography images acquired with a helical tomotherapy unit during image-guided radiation therapy. International Journal of Radiation Oncology Biology Physics, 2006, 65, 595-607.	0.4	68
70	Quantification of progression and regression of carotid vessel atherosclerosis using 3D ultrasound images. Annual International Conference of the IEEE Engineering in Medicine and Biology Society, 2006, , .	0.5	0
71	Evaluation of Segmentation algorithms for Medical Imaging. , 2005, 2005, 7186-9.		86
72	Prostate segmentation algorithm using dyadic wavelet transform and discrete dynamic contour. Physics in Medicine and Biology, 2004, 49, 4943-4960.	1.6	42